Title

Tissue-Specific Remodeling of the Mitochondrial Proteome in Type 1 Diabetic Akita Mice

Journal

Diabetes, 58(9)

ISSN

0012-1797

Authors

Bugger, Heiko
Chen, Dong
Riehle, Christian
et al.

Publication Date

2009-09-01

DOI

10.2337/db09-0259

Peer reviewed

Tissue-Specific Remodeling of the Mitochondrial Proteome in Type 1 Diabetic Akita Mice

Heiko Bugger,[1] Dong Chen,[2,3] Christian Riehle,[1] Jamie Soto,[1] Heather A. Theobald,[1] Xiao X. Hu,[1] Balasubramanian Ganesan,[2,3] Bart C. Weimer,[2,3] and E. Dale Abel[1]

OBJECTIVE—To elucidate the molecular basis for mitochondrial dysfunction, which has been implicated in the pathogenesis of diabetes complications.

RESEARCH DESIGN AND METHODS—Mitochondrial matrix and membrane fractions were generated from liver, brain, heart, and kidney of wild-type and type 1 diabetic Akita mice. Comparative proteomics was performed using label-free proteome expression analysis. Mitochondrial state 3 respirations and ATP synthesis were measured, and mitochondrial morphology was evaluated by electron microscopy. Expression of genes that regulate mitochondrial biogenesis, substrate utilization, and oxidative phosphorylation (OXPHOS) were determined.

RESULTS—In diabetic mice, fatty acid oxidation (FAO) proteins were less abundant in liver mitochondria, whereas FAO protein content was induced in mitochondria from all other tissues. Kidney mitochondria showed coordinate induction of tricarboxylic acid (TCA) cycle enzymes, whereas TCA cycle proteins were repressed in cardiac mitochondria. Levels of OXPHOS subunits were coordinately increased in liver mitochondria, whereas mitochondria of other tissues were unaffected. Mitochondrial respiration, ATP synthesis, and morphology were unaffected in liver and kidney mitochondria. In contrast, state 3 respirations, ATP synthesis, and mitochondrial cristae density were decreased in cardiac mitochondria and were accompanied by coordinate repression of OXPHOS and peroxisome proliferator–activated receptor (PPAR)-γ coactivator (PGC)-1α transcripts.

CONCLUSIONS—Type 1 diabetes causes tissue-specific remodeling of the mitochondrial proteome. Preservation of mitochondrial function in kidney, brain, and liver, versus mitochondrial dysfunction in the heart, supports a central role for mitochondrial dysfunction in diabetic cardiomyopathy. ***Diabetes*** **58: 1986–1997, 2009**

Type 1 diabetes reduces lifespan in affected humans, mainly because of complications such as cardiovascular disease and diabetic nephropathy (1,2). Substrate utilization is altered in several diabetic tissues. For example, myocardial fatty acid oxidation (FAO) and hepatic gluconeogenesis are increased (3,4). Changes in metabolite or hormone concentrations, such as reduced insulin and increased glucagon levels, may alter energy metabolism in diabetes. Moreover, activation of signaling cascades, such as the peroxisome proliferator–activated receptor (PPAR)-γ coactivator (PGC)-1α signaling pathway, may in turn modulate gene expression of oxidative phosphorylation (OXPHOS) proteins and enzymes of energy substrate metabolism (4–7). Several groups have investigated mitochondrial function in type 1 diabetic tissues, reporting mitochondrial oxidative stress and impairment of mitochondrial respiration and OXPHOS complex activities in various tissues (3,5,8–11). However, the molecular basis for the impairment in diabetes remains incompletely understood.

Gene expression profiling studies in liver and kidney tissue of type 1 diabetic rodents reveal significant associations between diabetes and changes in gene expression (12,13). Microarray analyses of cardiac tissue from streptozotocin-induced diabetic rats found 13% of 1,614 regulated genes encoding for mitochondrial proteins. Of note, expression of genes encoding FAO proteins were increased (14). Shen et al. (11) identified 20 significantly regulated myocardial proteins in type 1 diabetic OVE26 mice using two-dimensional gel electrophoresis, 12 of which were identified as mitochondrial proteins. Turko et al. (15) identified 30 regulated mitochondrial proteins when assessing cardiac mitochondrial proteins alone. They also observed increased mitochondrial FAO proteins and reduced content of a few OXPHOS protein subunits in myocardium of streptozotocin-induced diabetic rats. However, many mitochondrial proteins remained undetected in these studies due to the methodological limitations of gel-based comparative proteomics. Recently, Johnson et al. (16) used a semiquantitative liquid chromatography/mass spectrometry (LC/MS) approach to investigate whole-cell protein expression changes in liver and heart tissue of type 1 diabetic BB-DP rats. They reported 365 significantly regulated hepatic proteins in diabetic animals, a subset of which were mitochondrial proteins. While the dataset was used to generate hypotheses about diabetes-induced changes in liver metabolism, metabolic flux rates were not determined and patterns of protein expression were not compared between tissues (16). To our knowledge, no studies have systematically investigated differences in the mitochondrial proteome across

From the [1]Division of Endocrinology, Metabolism and Diabetes, and Program in Molecular Medicine, University of Utah School of Medicine, Salt Lake City, Utah; the [2]Department of Nutrition and Food Sciences, Utah State University, Logan, Utah; and the [3]Center for Integrated BioSystems, Utah State University, Logan, Utah.

Corresponding author: E. Dale Abel, dale.abel@hmbg.utah.edu.

Received 20 February 2009 and accepted 3 June 2009.

Published ahead of print at http://diabetes.diabetesjournals.org on 19 June 2009. DOI: 10.2337/db09-0259.

B.C.W. is currently affiliated with University of California Davis, School of Veterinary Medicine, Department of Population Health and Reproduction, Davis, California.

tissues in type 1 diabetes and related these to changes in mitochondrial function.

The hypothesis for this study is that mitochondrial dysfunction contributes to diabetes complications and that diabetes induces tissue-independent proteomic changes in mitochondria, thereby compromising mitochondrial function. Thus, we examined tissues in wild-type and type 1 diabetic Akita mice (Akita), which are known targets of diabetes complications, namely cardiac, renal, and brain tissue. Liver mitochondria were also examined to determine whether changes in mitochondrial function and proteins were uniform across multiple tissues. Akita mice are a genetic model of type 1 diabetes that circumvent potential extrapancreatic toxic effects of streptozotocin and still develop many typical diabetes complications (17,18). To increase protein coverage beyond gel-based approaches, we fractionated mitochondria into matrix and membrane fractions and analyzed the protein composition directly using protein expression analysis with LC-tandem MS (LC-MS/MS). The proteome of each tissue was complemented by measurement of respiratory function in isolated mitochondria, evaluation of mitochondrial morphology, and gene expression analysis for regulators of mitochondrial biogenesis, substrate utilization, and oxidative phosphorylation. We found that type 1 diabetes leads to remodeling of the proteome that regulates mitochondrial energy metabolism with distinct changes in each tissue examined. However, mitochondrial dysfunction was only evident in the heart, suggesting increased susceptibility of cardiac mitochondria to diabetes-induced dysfunction.

RESEARCH DESIGN AND METHODS

Male heterozygous Ins2$^{+/-}$ Akita mice (C57BL/6) and C57BL/6 controls were obtained from The Jackson Laboratories (Bar Harbor, ME), were housed at 22°C, were given free access to water and food, had a light cycle of 12 h light and 12 h dark, and were studied at the age of 12 weeks. Animals were studied in accordance with protocols approved by the institutional animal care and use committee of the University of Utah.

Mitochondrial isolation. Livers, hearts, brains, and kidneys were removed from chloral hydrate–anesthetized animals (1 mg/g body wt) and placed immediately in ice-cold STE1 buffer (250 mmol/l sucrose, 5 mmol/l Tris/HCl, 2 mmol/l EGTA, pH 7.4). In one set of experiments, heart and kidneys were excised from the same mouse (within 20 s of anesthesia), and in another set of experiments, brain and liver were excised from the same mouse (within 30 s of anesthesia). Organs that had to be pooled from different animals were kept in ice-cold STE1 buffer (<5 min) until sufficient numbers of organs were harvested. Four hearts were pooled, minced, incubated in 2.5 ml STE2 buffer (STE1 containing [wt/vol] 0.5% BSA, 5 mmol/l $MgCl_2$, 1 mmol/l ATP, and 2.5 units/ml protease type VIII from *Bacillus licheniformis*) for 4 min, diluted with 2.5 ml STE1 buffer, and homogenized using a Teflon pistil in a Potter-Elvejhem glass homogenizer. The homogenate was further diluted with 5 ml STE1 containing one tablet Complete Mini protease inhibitor cocktail (Roche, Indianapolis, IN). Similar to hearts, two kidneys (pooled) or one liver were minced, homogenized in 5 ml STE1 buffer, and further diluted with 5 ml STE1 containing one tablet Complete Mini. Four brains (pooled) were minced, homogenized in 5 ml isolation medium (250 mmol/l sucrose, 1 mmol/l EDTA, 1 mg/ml BSA, and 0.25 mmol/l dithiothreitol, pH 7.4), and diluted by adding 5 ml isolation medium containing one tablet of Complete Mini. Heart homogenates were centrifuged at 8,000*g* for 10 min, and the resulting pellet was resuspended in STE1 buffer and centrifuged at 700*g* for 10 min. The resulting supernatant was centrifuged twice at 8,000*g* for 10 min. Kidney or liver homogenates were centrifuged at 1,000*g* for 5 min, and the resulting supernatant was centrifuged twice at 10,000*g* for 10 min. Brain homogenates were centrifuged at 500*g* for 5 min in four separate tubes. Resulting supernatants were centrifuged at 15,000*g* for 5 min; each pellet was resuspended in 150 μl isolation medium, loaded on a Percoll gradient (0.6 ml 23%, 0.6 ml 15%, 0.6 ml 10%, and 0.6 ml 3% Percoll solution), and centrifuged in a swinging-bucket rotor (Beckman SW55Ti) at 32,500*g* for 8 min. The nonsynaptic mitochondrial pellet (bottom layer) was collected, resuspended in 2.5 ml isolation medium, and centrifuged twice at 10,000*g* for 10 min. The pellet obtained from each mitochondrial isolation was resuspended in 1 ml buffer B (250 mmol/l sucrose, 1 mmol/l EDTA, 10 mmol/l Tris/HCl, pH 7.4). All centrifugation steps were carried out at 4°C.

Mitochondrial purification and fractionation. Mitochondrial isolates were loaded on a Percoll gradient (2.2 ml 2.5 mol/l sucrose, 6.55 ml Percoll, 12.25 ml TE [10 mmol/l Tris/HCl, 1 mmol/l EDTA, pH 7.4]) and centrifuged at 60,000*g* for 45 min at 4°C as described by Hovius et al. (19). The lower layer was resuspended in 5 ml of buffer B and centrifuged three times at 10,000*g* for 10 min at 4°C. The pellet was resuspended in 100 μl 10 mmol/l Tris/HCl, pH 8.5, and freeze-thawed three times (5 min liquid nitrogen/5 min 37°C water bath). Fractionation was achieved by centrifuging the isolate at 40,000*g* for 20 min at 4°C. Centrifugation was repeated for the respective supernatant (matrix) and pellet (membrane) fractions to reduce membrane or matrix protein cross-contamination. Protein concentrations were determined using the Micro BCA Protein Assay Kit (Pierce, Rockford, IL).

Protein in-solution tryptic digestion. A total of 5 μl of 0.2% RapidGest (Waters, Manchester, U.K.) was added to 20 μg of membrane protein sample in 15 μl H_2O. The mixed solution was heated at 80°C for 20 min, and the protein mixtures were tryptically digested as described by the Waters Protein Expression System Manual (Waters 2006). After adding NH_4HCO_3 and treatment with dithiothreitol and iodoacetamide, 4 μl of 0.11 μg/μl trypsin in 25 mmol/l NH_4HCO_3 was added to the protein sample. Samples were incubated at 37°C overnight, incubated with 1% formic acid for 30 min at 37°C, and centrifuged at 10,000*g* for 10 min. The supernatant was used to determine the proteome.

Protein expression. Equal amounts of digested protein in a final volume of 3 μl were introduced into a Symmetry C18 trapping column (180 μmol/l × 20 mm) with the NanoACQUITY Sample Manager (Waters) and washed with H_2O for 2 min at 10 ml/min. Using solvent A (99.9% H_2O and 0.1% formic acid) and solvent B (99.9% acetonitrile and 0.1% formic acid), the peptides were eluted from the trapping column over a 100-μm × 100-mm BEH 130 C18 column with a 140-min gradient (1–4% B for 0.1 min, 4–25% B for 89.9 min, 25–35% B for 5 min, 35–85% B for 2 min, 85% B for 13 min, 85–95% B for 8 min, 95–1% B for 2 min, and 1% B for 20 min) at 0.8 μl/min flow rate using a NanoACQUITY UPLC (Waters). The mass spectrometer (MS), Q-TOF Premier (Waters), was set to a parallel fragmentation mode with scan times of 1.0 s. The low fragmentation energy was 5 V and the high fragmentation energy was 17–45 V. Fibrinopeptide B (GLU1) was used as the external calibration standard with LockSpray. Enolase was used as the internal control. MS spectra were analyzed by Waters ProteinLynx Global Server 2.3. The following default setting was used for protein identification: minimum peptide matches per protein, 1; minimum fragment ion matches per peptide, 3; minimum fragment ion matches per protein, 7; and the protein false-positive discovery rate, 4%. The database search algorithm of Waters ProteinLynx Global Server 2.3 was described by Levin et al. (20). Gene ontology enrichment analysis was performed using Bioconductor as described before (21). Analyses were performed on the proteomic dataset of matrix or membrane fractions of liver, brain, heart, or kidney mitochondria or in matrix or membrane fractions across all tissues. Gene ontology terms were considered significantly enriched between wild-type and Akita mice if $P < 0.05$. Canonical pathway analysis was performed using ingenuity pathways analysis (IPA) (Ingenuity Systems, Redwood City, CA).

Gene expression analysis. Total RNA was extracted from livers, hearts, brains, and kidneys with Trizol (Invitrogen, Carlsbad, CA), purified with the RNEasy Kit (Qiagen, Valencia, CA) and reverse transcribed (3). Equal amounts of cDNA were subjected to quantitative real-time RT-PCR using SYBR Green as a probe. Data were normalized by comparison to the invariant transcript 16S RNA. Primer sequences are presented in online appendix Table S17 (available at http://diabetes.diabetesjournals.org/cgi/content/full/db09-0259/DC1).

Mitochondrial function. Mitochondria were isolated, as described above, without addition of protease inhibitors and incubated in respiration medium (120 mmol/l KCl, 5 mmol/l KH_2PO_4, 1 mmol/l EGTA, 1 mg/ml BSA, and 3 mmol/l HEPES, pH 7.2, 25°C) containing 5 mmol/l succinate/10 μmol/l rotenone or 5 mmol/l glutamate/2 mmol/l malate or 20 μmol/l palmitoylcarnitine/2 mmol/l malate. State 2 respiration was measured in the presence of substrate only, state 3 respiration after addition of adenosine diphosphate (ADP; 1 mmol/l), and state 4 respiration following complete utilization of the added ADP. In separate experiments, the uncoupling agent carbonyl cyanide p-trifluoromethoxyphenylhydrazone (FCCP; 1 μmol/l) was added following addition of ADP in the presence of succinate/rotenone or glutamate/malate as substrates. ATP synthesis was measured by incubating mitochondria in respiration medium containing substrates at 25°C. A total of 1 mmol/l ADP was added, and samples were collected at 10-s intervals following ADP addition for a total of 60 s. ATP content of the samples was analyzed using a luminometric assay as previously described (22). Mitochondrial hydrogen peroxide (H_2O_2) generation was measured using succinate as a substrate as previously described (3). To block H_2O_2 production at complex I, 10 μmol/l

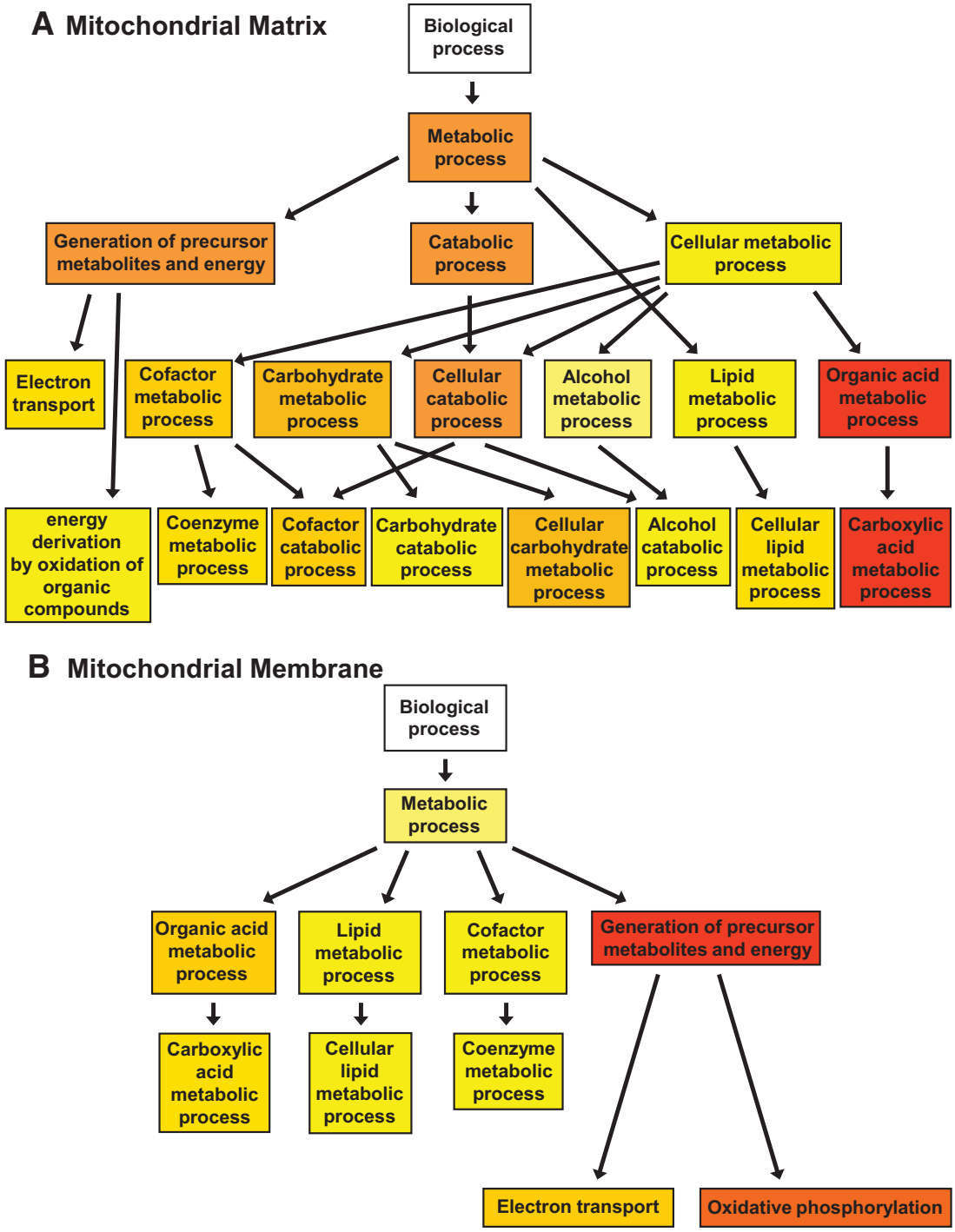

FIG. 1. GO enrichment analysis. Simplified hierarchical trees of selected GO terms (*boxes*) of the "biological process" category that are enriched to the greatest extent in matrix (*A*) or membrane (*B*) fractions of Akita mitochondria using pooled proteomic data from all tissues (complete GO enrichment analyses are presented in online appendix Tables S4 and S5). Significantly enriched GO terms ($P < 0.05$) are highlighted, and the degree of color saturation of each node positively correlates with the enrichment significance of the corresponding GO term (red = most significant enrichment).

rotenone was added to the reaction. This assay is widely accepted as a measure of mitochondrial superoxide production.

Tissue ultrastructure. Tissues were freshly excised, immediately washed in ice-cold saline, and processed for electron microscopy analysis as previously described (22). Mitochondrial volume density and number were analyzed by stereology in a blinded fashion using the point-counting method (22,23).

Statistical analysis. Data are presented as means ± SE. Statistical analysis of proteomic data were performed using the Waters ProteinLynx Global Server version 2.3 software using a clustering algorithm, which chemically clusters peptide components by mass and retention time for all injected samples and performs binary comparisons for each experimental condition to generate an average normalized intensity ratio for all matched AMRT (accurate mass, retention time) components. The Student's *t* test was used for each binary comparison. Respiration, stereology, and gene expression data were analyzed with Student's *t* test using StatView 5.0.1 (SAS Institute, Cary, NC). Significant differences were accepted at $P < 0.05$.

RESULTS

Mitochondrial protein yields. Akita mice develop severe diabetes at 5–6 weeks of age (18) and were studied at

TABLE 1
Abundance of FAO proteins, TCA cycle enzymes, and OXPHOS subunits in mitochondria of liver, brain, heart, and kidney of Akita, presented as fold change compared with wild type

Protein	Liver	Brain	Heart	Kidney
FAO				
Acyl-coenzyme A acyltransferase 2 (mitochondrial 3-oxoacyl-coenzyme A thiolase)	0.75*	1.27†	1.41†	1.69†
Acyl-coenzyme A dehydrogenase, long chain	0.89	1.25†	1.14†	1.18†
Acyl-coenzyme A dehydrogenase, medium chain	0.96	1.12	1.03	0.94
Acyl-coenzyme A dehydrogenase, short chain	0.76*	1.45	1.11	1.03
Carnitine O-octanoyltransferase	0.70	ND	ND	0.68*
Dodecenoyl-coenzyme A δ isomerase (3,2 trans-enoyl-coenyme A isomerase)	0.83*	1.14	1.11	1.32†
Enoyl coenzyme A hydratase, short chain, 1, mitochondrial	1.05	1.00	0.94	1.01
Hydroxyacyl-coenzyme A dehydrogenase/3-ketoacyl-coenzyme A thiolase/enoyl-coenzyme A hydratase (trifunctional protein), α-subunit	1.16	1.33	1.20†	1.52†
TCA cycle				
Aconitase 2, mitochondrial	1.07	1.00	0.96	1.32†
Citrate synthase	0.93	0.97	0.86*	1.25†
Fumarate hydratase 1	1.02	1.04	0.90	1.08
Isocitrate dehydrogenase 3 (NAD^+) α	ND	0.87*	0.88*	1.52†
Isocitrate dehydrogenase 3, β-subunit	ND	1.02	1.20	1.15
Malate dehydrogenase 2, NAD (mitochondrial)	0.91	0.97	0.76*	1.30†
Succinate-CoA ligase, GDP forming, α-subunit	1.03	0.89	1.19	1.18†
Succinate-coenzyme A ligase, ADP forming, β-subunit	0.93	0.89	1.00	1.22†
Succinate dehydrogenase Fp subunit	1.15	1.05	0.90	0.98
Succinate dehydrogenase Ip subunit	1.19	0.98	0.96	1.01
Oxidative phosphorylation				
ATPase, H +/K + transporting, nongastric, α polypeptide	ND	0.98	ND	ND
ATP synthase, H + transporting, mitochondrial F1 complex, α-subunit, isoform 1	1.22†	1.11†	0.99	1.00
ATP synthase, H + transporting mitochondrial F1 complex, β-subunit	1.23†	1.03	1.09†	1.01
ATP synthase, H + transporting, mitochondrial F1 complex, δ-subunit precursor	0.70*	0.88	ND	0.94
ATP synthase, H + transporting, mitochondrial F1 complex, γ-subunit	1.02	1.08	1.11	1.00
ATP synthase, H + transporting, mitochondrial F1 complex, O-subunit	1.27†	0.97	0.98	1.05
ATP synthase, H + transporting, mitochondrial F0 complex, subunit b, isoform 1	1.11	0.99	1.00	0.98
ATP synthase, H + transporting, mitochondrial F0 complex, subunit d	1.49†	0.95	1.03	1.04
ATP synthase, H + transporting, mitochondrial F0 complex, subunit F	1.41†	1.28†	1.04	1.03
Cytochrome c oxidase subunit II	1.18	1.00	0.84*	1.11
Cytochrome c oxidase subunit IV isoform 1	1.32†	1.01	1.11	1.09
Cytochrome c oxidase, subunit Va	1.32†	0.82	0.89	1.08
Cytochrome c oxidase, subunit VIb polypeptide 1	1.15	1.11	0.95	1.01
Cytochrome c oxidase, subunit VIIa 1	ND	ND	0.95	ND
NADH dehydrogenase (ubiquinone) 1 α subcomplex 10	1.33†	1.03	0.76*	1.22†
NADH dehydrogenase (ubiquinone) 1 α subcomplex, 4	1.19†	1.06	1.03	1.04
NADH dehydrogenase (ubiquinone) 1 α subcomplex, 8	ND	0.99	0.99	0.97
NADH dehydrogenase (ubiquinone) 1 α subcomplex, 9	1.56†	0.90	0.93	1.01
NADH dehydrogenase (ubiquinone) 1 β subcomplex, 10	2.22†	0.88	0.82	1.19
NADH dehydrogenase (ubiquinone) Fe-S protein 1	1.18	1.01	0.84*	1.11
NADH dehydrogenase (ubiquinone) Fe-S protein 2	1.54†	0.93	0.92	1.05
NADH dehydrogenase (ubiquinone) flavoprotein 1	1.37†	0.99	0.87	1.09
Predicted: similar to ATP synthase coupling factor 6, mitochondrial precursor (ATPase subunit F6)	1.25	1.16	1.04	1.03
Predicted: similar to NADH dehydrogenase (ubiquinone) Fe-S protein 6	ND	1.11	0.95	1.28
Ubiquinol-cytochrome c reductase core protein 1	1.10	0.99	0.88	1.05
Ubiquinol cytochrome c reductase core protein 2	1.12†	0.96	0.92	1.01
Ubiquinol-cytochrome c reductase binding protein	0.84	0.92	1.09	0.98
Ubiquinol-cytochrome c reductase, Rieske iron-sulfur polypeptide 1	1.15	1.01	0.93	1.10
Succinate dehydrogenase Fp subunit	1.15	1.05	0.90	0.98
Succinate dehydrogenase Ip subunit	1.19	0.98	0.96	1.01

*Significantly downregulated proteins. †Significantly upregulated proteins. Symbols indicate a significant difference ($P < 0.05$) compared with wild type. ND, protein was not detected.

the age of 12 weeks. On the day they were killed, Akita mice were severely hyperglycemic (560 ± 16 vs. 162 ± 10 mg/dl; $P < 0.05$) and were hypertriglyceridemic (114 ± 9 vs. 58 ± 3 mg/dl; $P < 0.05$). Relative changes in protein abundance between wild-type and Akita mitochondrial fractions were determined using LC-MS/MS. A total of 218 proteins in liver mitochondria (matrix 83, membrane 135), 295 proteins in brain mitochondria (matrix 154, membrane 141), 123 proteins in cardiac mitochondria (matrix 54, membrane 69), and 186 proteins in kidney mitochondria (matrix 87, membrane 99) were identified (supplementary Table S1). Of all matrix fractions, kidney mitochondria showed the greatest number of proteins with significant changes in mitochondrial protein content

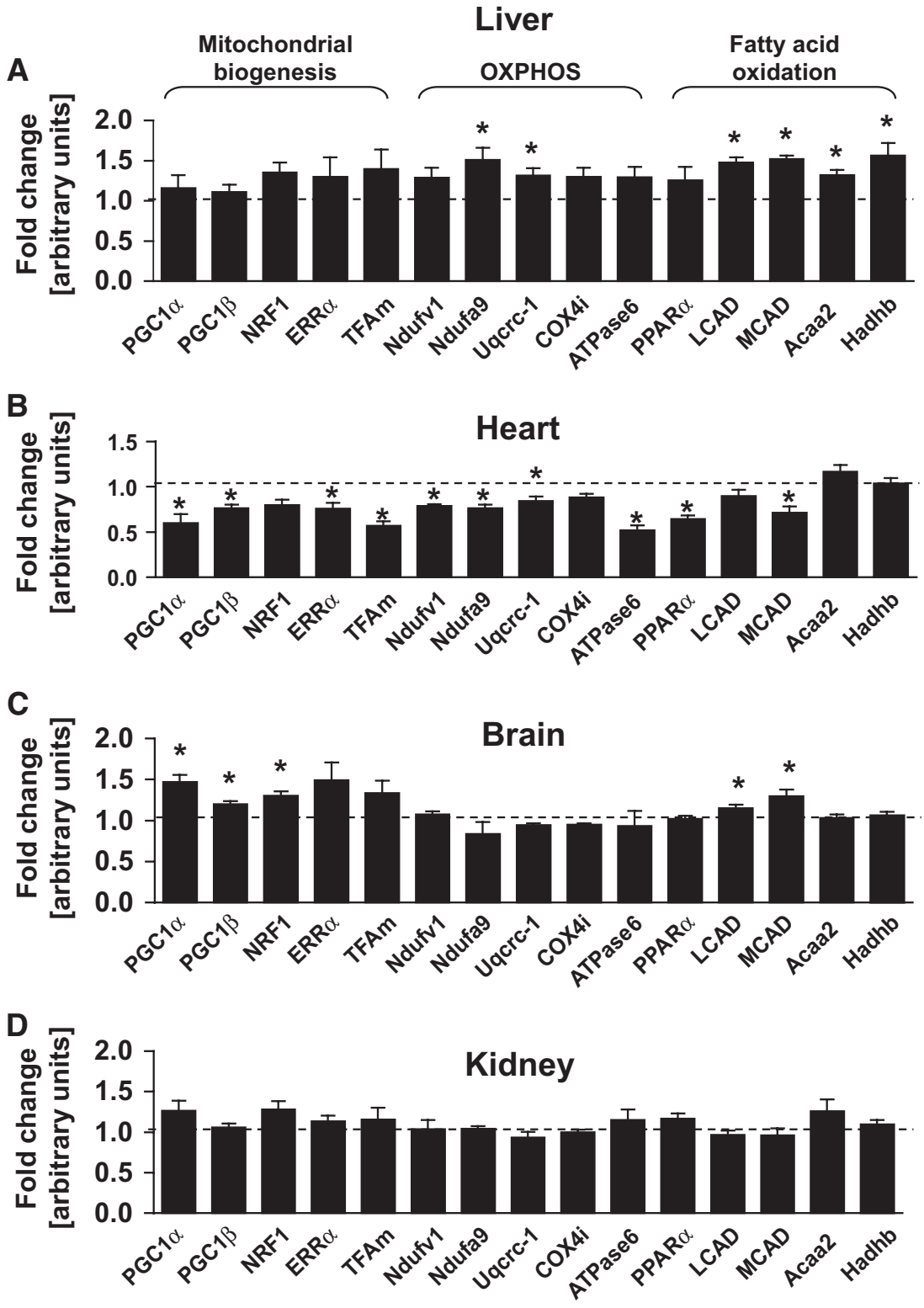

FIG. 2. Gene expression. Gene expression in liver (*A*), heart (*B*), brain (*C*), and kidney (*D*) tissue of 12-week-old wild-type and Akita mice normalized to 16S RNA transcript levels (n = 6–8). Values represent fold change in mRNA transcript levels relative to wild type, which was assigned as one (dashed line).

compared with wild type (52%). Of all membrane fractions, liver mitochondria showed the greatest number of proteins with significant changes in mitochondrial protein content compared with wild type (42%). Matrix and membrane fractions of brain mitochondria exhibited the lowest number of diabetes-related changes in protein content (13% in each fraction). Proteins were analyzed by gene ontology (GO) term enrichment analysis (supplementary Tables S2 and S3 and supplementary Figs. S4–S13) and were also sorted by canonical pathway annotation using the IPA software (supplementary Tables S14 and S15).

TABLE 2
Comparison of gene expression and mitochondrial protein abundance of selected OXPHOS and FAO proteins in liver, brain, heart, and kidney tissue obtained from wild-type and Akita mice, presented as fold change relative with wild type

	Gene	Protein
Liver		
Oxidative phosphorylation		
NADH dehydrogenase (ubiquinone) flavoprotein 1	1.29	1.37†
NADH dehydrogenase (ubiquinone) 1 α subcomplex, 9	1.51†	1.56†
Ubiquinol-cytochrome c reductase core protein 1	1.31†	1.10
Cytochrome c oxidase subunit IV isoform 1	1.30	1.32†
ATP synthase coupling factor 6 (ATPase subunit F6)	1.29	1.25
FAO		
Acyl-coenzyme A dehydrogenase, medium chain	1.52†	0.96
Acyl-coenzyme A dehydrogenase, long chain	1.48†	0.89
Acyl-coenzyme A acyltransferase 2	1.32†	0.75*
Brain		
Oxidative phosphorylation		
NADH dehydrogenase (ubiquinone) flavoprotein 1	1.07	0.99
NADH dehydrogenase (ubiquinone) 1 α subcomplex, 9	0.83	0.90
Ubiquinol-cytochrome c reductase core protein 1	0.94	0.99
Cytochrome c oxidase subunit IV isoform 1	0.95	1.01
ATP synthase coupling factor 6 (ATPase subunit F6)	0.93	1.16
FAO		
Acyl-coenzyme A dehydrogenase, medium chain	1.30†	1.12
Acyl-coenzyme A dehydrogenase, long chain	1.15†	1.25†
Acyl-coenzyme A acyltransferase 2	1.03	1.27†
Heart		
Oxidative phosphorylation		
NADH dehydrogenase (ubiquinone) flavoprotein 1	0.79*	0.87
NADH dehydrogenase (ubiquinone) 1 α subcomplex, 9	0.76*	0.93
Ubiquinol-cytochrome c reductase core protein 1	0.84*	0.88
Cytochrome c oxidase subunit IV isoform 1	0.88	1.11
ATP synthase coupling factor 6 (ATPase subunit F6)	0.52*	1.04
FAO		
Acyl-coenzyme A dehydrogenase, medium chain	0.71*	1.03
Acyl-coenzyme A dehydrogenase, long chain	0.90	1.14†
Acyl-coenzyme A acyltransferase 2	1.17	1.41†
Kidney		
Oxidative phosphorylation		
NADH dehydrogenase (ubiquinone) flavoprotein 1	1.04	1.09
NADH dehydrogenase (ubiquinone) 1 α subcomplex, 9	1.04	1.01
Ubiquinol-cytochrome c reductase core protein 1	0.93	1.05
Cytochrome c oxidase subunit IV isoform 1	0.99	1.09
ATP synthase coupling factor 6 (ATPase subunit F6)	1.15	1.03
FAO		
Acyl-coenzyme A dehydrogenase, medium chain	0.96	0.94
Acyl-coenzyme A dehydrogenase, long chain	0.96	1.18†
Acyl-coenzyme A acyltransferase 2	1.26	1.69†

*Significantly downregulated gene/protein. †Significantly upregulated gene/protein. Symbols indicate a significant difference ($P < 0.05$) compared with wild type.

GO term enrichment analysis. To identify biological processes that were altered in Akita mitochondria, we performed a GO term enrichment analysis on the entire proteomic dataset (pooled from all tissues) in matrix and membrane fractions, respectively (supplementary Figs. S4 and S5). We generated simplified GO term enrichment trees for matrix (Fig. 1*A*) and membrane (Fig. 1*B*) fractions in the "biological process" category and illustrate the highly enriched GO terms in Fig. 1. GO terms for energy metabolic processes were highly enriched in mitochondrial matrix fractions of Akita mice, including lipid and carboxylic acid metabolism, carbohydrate metabolism, and electron transport (Fig. 1*A*). In contrast, other GO terms, such as response to oxidative stress, were less enriched (supplementary Fig. S4). GO terms of metabolic processes were also enriched in membrane fractions of Akita mitochondria, particularly energy generation and oxidative phosphorylation (Fig. 1*B*). Thus, we focused further on mitochondrial energy metabolic pathways, investigating each organ for common and unique diabetes-related changes. The proteomic datasets of each tissue were subjected to canonical pathway analysis using the IPA software (supplementary Tables S14 and S15), and selected energy metabolic pathways are presented in Table 1.

Proteins of FAO. FAO proteins were significantly regulated in Akita mitochondria in all tissues (Table 1). Of the identified proteins, three of eight FAO proteins were significantly repressed in liver mitochondria, and all but two of the remaining FAO proteins were less than wild

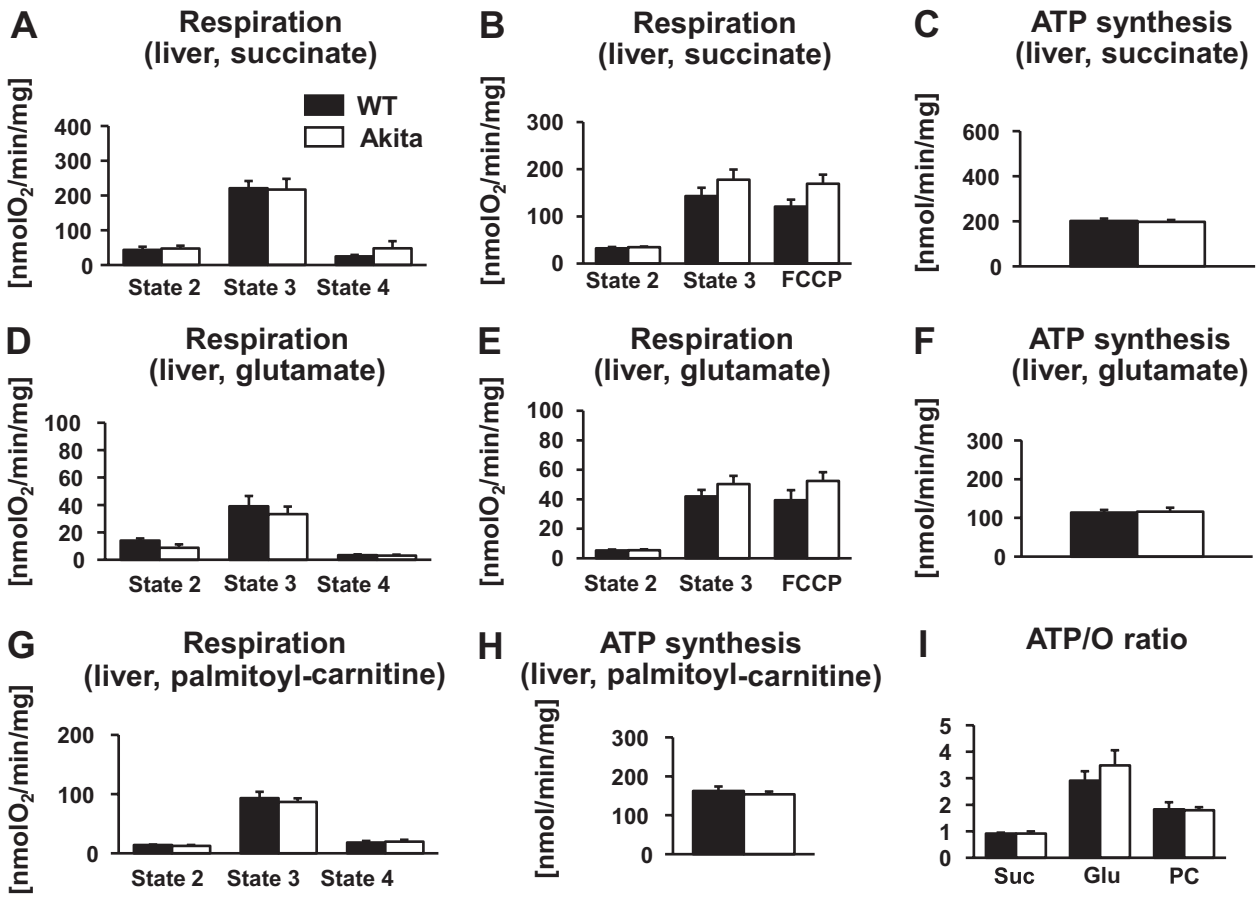

FIG. 3. Mitochondrial function in the liver. Respiration rates (*A*, *B*, *D*, *E*, and *G*) and ATP synthesis rates (*C*, *F*, and *H*) of mitochondria isolated from livers of 12-week-old wild-type (WT) (■) and Akita (□) mice, measured in the presence of succinate/rotenone (*A–C*) or glutamate/malate (*D–F*) or palmitoyl-carnitine/malate (*G* and *H*) as a substrate (n = 5–7). *I*: State 3 respiration and ATP synthesis rates were used to calculate ATP-to-O ratios for each substrate. There were no significant differences in any parameter. glu, glutamate; pc, palmitoyl-carnitine; suc, succinate.

type. In contrast, two of seven FAO proteins were significantly induced in brain mitochondria and the remaining proteins were uniformly greater than wild type. In cardiac mitochondria, three of seven FAO proteins were significantly induced, and with one exception the remaining proteins were greater than wild type. In kidney mitochondria of Akita, four of eight FAO proteins were significantly induced, while only one protein was significantly repressed.

Proteins of the tricarboxylic acid cycle. Tricarboxylic acid (TCA) cycle proteins were coordinately induced in kidney mitochondria of Akita (6 of 10 proteins) (Table 1). In contrast, 3 of 10 TCA cycle proteins (citrate synthase, isocitrate dehydrogenase 3 [NAD^+] α, and malate dehydrogenase 2) were significantly repressed in cardiac mitochondria, and of the remaining proteins only one was greater than wild-type levels. In liver and brain mitochondria, TCA cycle proteins were unaffected by diabetes, with no significantly regulated proteins in liver mitochondria. Only one TCA protein, isocitrate dehydrogenase 3 (NAD^+) α, was significantly repressed in brain mitochondria of Akita mice.

Proteins of oxidative phosphorylation. Protein levels of OXPHOS subunits were coordinately induced in liver mitochondria of Akita mice (14 of 26 proteins), including subunits of complexes I, II, III, and IV (Table 1). In contrast, three OXPHOS subunits were significantly repressed in cardiac mitochondria, and of the remaining 24 proteins, 67% were lower than wild-type levels. In brain and kidney mitochondria, OXPHOS subunits were generally not regulated. Only 2 of 29 OXPHOS subunits were significantly increased in brain mitochondria, and only 1 of 28 OXPHOS subunits was significantly increased in kidney mitochondria of Akita.

Expression of nuclear-encoded mitochondrial genes. We determined if diabetes-induced transcriptional changes of energy metabolism enzymes predicted mitochondrial protein composition in each tissue. In liver, expression of FAO and OXPHOS genes increased, but their transcriptional regulators did not (Fig. 2*A*). Thus, OXPHOS gene expression mirrored proteomic changes in liver mitochondria, but the direction of change in FAO gene expression was discordant with protein changes. This observation is illustrated in Table 2, which compares the expression levels of investigated FAO and OXPHOS genes with their respective mitochondrial protein levels. In contrast, gene expression was generally reduced in cardiac tissue (Fig. 2*B*). Expression of OXPHOS subunit genes and the FAO protein medium-chain acyl CoA dehydrogenase was significantly reduced. These transcriptional changes were accompanied by reduced expression of *PGC-1*α, *PGC-1*β, estrogen-related receptor α, mitochondrial transcription factor-A, and *PPAR*α. Thus, OXPHOS gene expression mirrored proteomic changes in heart mitochondria, but the direction of change in FAO gene expression was discordant with the change in mitochondrial FAO proteins (Table 2). In the brain, expression of *PGC-1*α, *PGC-1*β, and nuclear respiratory factor-1 was increased; however, none of the OXPHOS genes were induced (Fig. 2*C*). With respect to FAO, *PPAR*α expression was unchanged, but

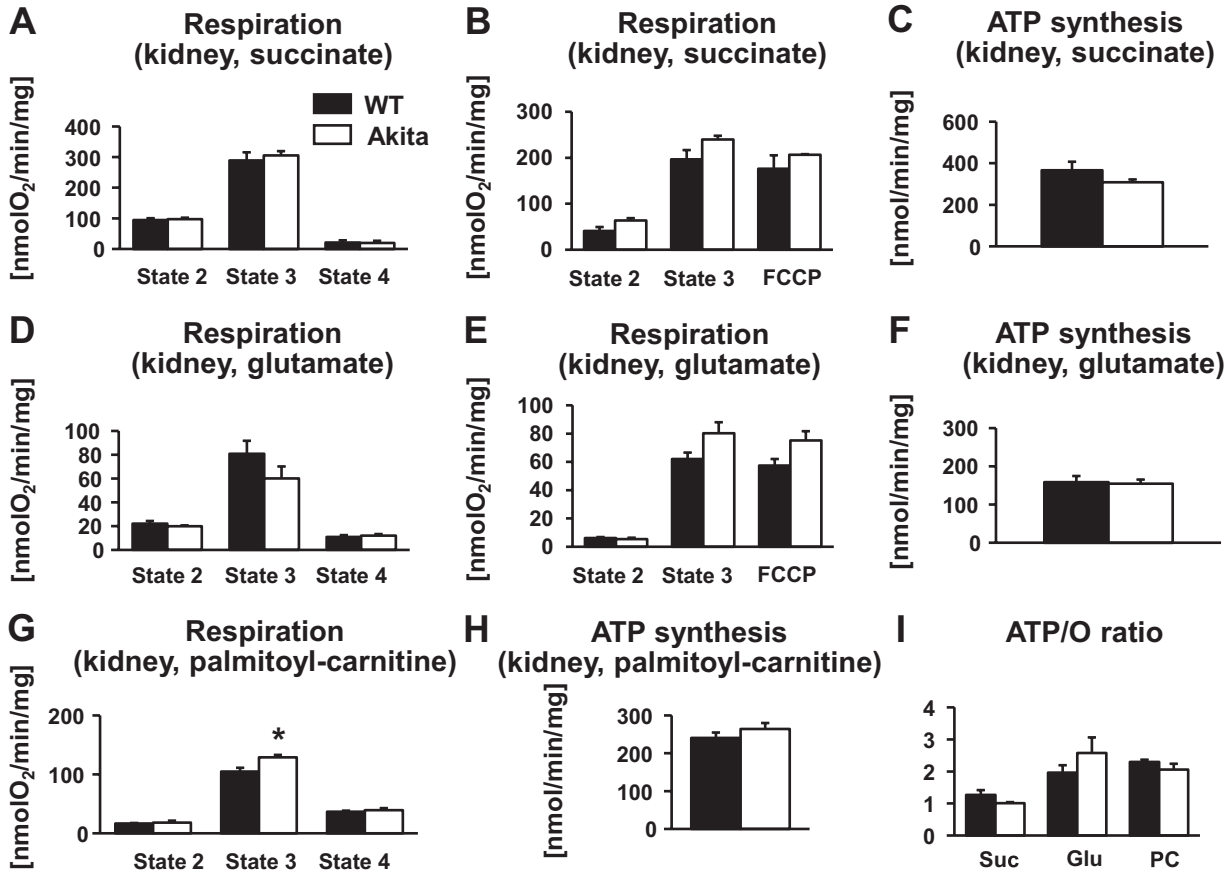

FIG. 4. Mitochondrial function in the kidney. Respiration rates (*A*, *B*, *D*, *E*, and *G*) and ATP synthesis rates (*C*, *F*, and *H*) of mitochondria isolated from kidneys of 12-week-old wild-type (WT) (■) and Akita (□) mice, measured in the presence of succinate/rotenone (*A–C*) or glutamate/malate (*D–F*) or palmitoyl-carnitine/malate (*G* and *H*) as a substrate (n = 5–7). *I*: State 3 respiration and ATP synthesis rates were used to calculate ATP-to-O ratios for each substrate. *P < 0.05 vs. wild type. glu, glutamate; pc, palmitoyl-carnitine; suc, succinate.

expression of two FAO genes increased. Thus, the brain was the only tissue in which changes in FAO gene expression tended to mirror changes in the mitochondrial proteome (Table 2). Despite the large number of regulated proteins in kidney mitochondria, expression levels of the genes investigated were not significantly different between wild-type and Akita kidneys (Fig. 2*D*). In summary, with the exception of the brain, gene expression changes did not predict changes in FAO proteins, whereas trends in OXPHOS gene expression paralleled mitochondrial OXPHOS subunit protein content in all tissues.

Mitochondrial function. The TCA cycle and the respiratory chain are important determinants of mitochondrial respiratory function, and proteins of these energy metabolic pathways were significantly regulated in Akita liver, heart, and kidney mitochondria. We therefore measured mitochondrial respiration rates and ATP synthesis in isolated mitochondria. Despite a coordinate induction of OXPHOS subunits in liver mitochondria and a coordinate induction of TCA cycle proteins in kidney mitochondria of Akita, both state 3 respiration and ATP synthesis were unchanged in both tissues, using succinate or glutamate as the substrate (Fig. 3*A*, *C*, *D*, and *F* and Fig. 4*A*, *C*, *D*, and *F*). These findings were confirmed in respiration measurements in which oxygen consumption was stimulated with the uncoupling agent FCCP, both using succinate or glutamate as substrates (Fig. 3*B* and *E* and Fig. 4*B* and *E*). Mitochondrial function was also not enhanced in these tissues using palmitoyl-carnitine as a substrate, except for a significant increase in state 3 respiration in kidney mitochondria of Akita mice (Fig. 3*G* and *H* and Fig. 4*G* and *H*). In contrast, state 3 respiration, FCCP-stimulated respiration, and ATP synthesis were reduced in cardiac mitochondria of Akita mice, both with glutamate and succinate as a substrate (Fig. 5*A–F*). ATP-to-O ratios were not different in liver, kidney, or heart mitochondria with any substrate (Fig. 3*I* and Fig. 4*I* and Fig. 5*G*).

Because we observed decreased mitochondrial H_2O_2 production in Akita hearts in our previous study (3), we also measured H_2O_2 generation in mitochondria obtained from liver and kidney tissues of wild-type and Akita mice. In liver mitochondria, succinate-driven H_2O_2 production was markedly decreased in Akita mice (supplementary Fig. S16*A*). In kidney mitochondria, H_2O_2 production was not different between the groups (supplementary Fig. S16*B*). In mitochondria of wild-type and Akita mice, hepatic and renal H_2O_2 generation were markedly decreased following addition of the complex I inhibitor rotenone.

Tissue ultrastructure. We recently reported altered mitochondrial morphology in hearts of 24-week-old Akita mice, characterized by markedly reduced cristae density and increased mitochondrial volume density (3). Therefore, we also evaluated mitochondrial morphology in liver, brain, heart, and kidney tissues of 12-week-old Akita mice in this study. Mitochondrial morphology was not different between wild-type and Akita mice in liver, brain, and kidney tissue (Fig. 6*A–C*). However, mitochondrial cristae density was clearly reduced in cardiac tissue of Akita mice (Fig. 6*D*).

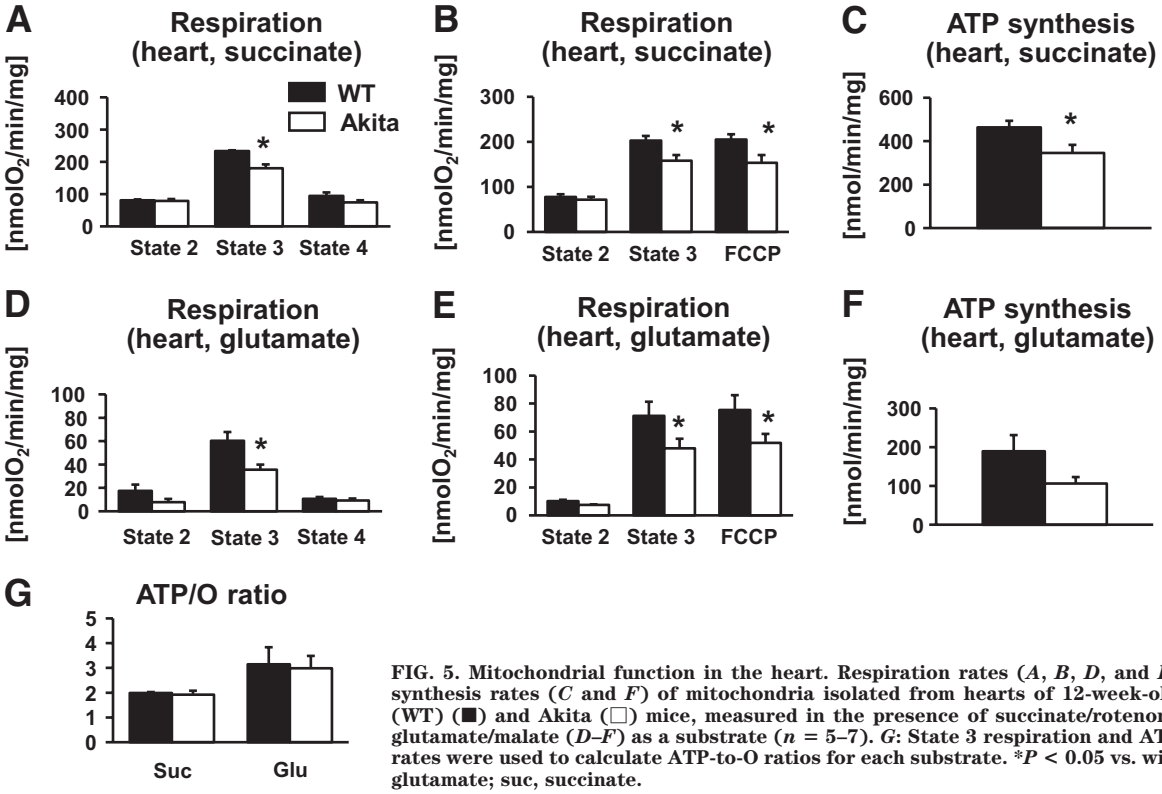

FIG. 5. Mitochondrial function in the heart. Respiration rates (*A*, *B*, *D*, and *E*) and ATP synthesis rates (*C* and *F*) of mitochondria isolated from hearts of 12-week-old wild-type (WT) (■) and Akita (□) mice, measured in the presence of succinate/rotenone (*A–C*) or glutamate/malate (*D–F*) as a substrate (n = 5–7). *G*: State 3 respiration and ATP synthesis rates were used to calculate ATP-to-O ratios for each substrate. *$P < 0.05$ vs. wild type. glu, glutamate; suc, succinate.

Mitochondrial volume density and mitochondrial number in kidney and liver tissue, quantified by stereology, were not different between wild-type and Akita mice (Fig. 6*E* and *F*). In contrast, both mitochondrial volume density and number were increased in Akita hearts (Fig. 6*E* and *F*).

DISCUSSION

In the present study, we show that type 1 diabetes causes tissue-specific remodeling of the proteome involved in mitochondrial energy metabolism. The hepatic mitochondrial proteome was regulated to the greatest extent (41% of all identified proteins), and the cerebral mitochondrial proteome was regulated the least (13%). The tissue-specific remodeling is not surprising, considering that the mitochondrial proteome composition is quite different among tissues, even in normal animals (24,25). The fact that proteins of substrate metabolism were regulated to the greatest extent in liver mitochondria of Akita appears plausible, since the liver plays a central role in the regulation of systemic glucose metabolism, such as maintenance of glucose concentrations by modulating gluconeogenesis under fed and fasted conditions (26). Thus, hepatic energy metabolism may be particularly sensitive to diabetes-associated changes in systemic concentrations of glucose and insulin.

With the exception of the brain, mitochondrial FAO protein levels did not parallel FAO gene expression in Akita mice. In the liver, FAO gene expression was increased, whereas mitochondrial FAO protein content was reduced. Similarly, FAO gene expression was reduced but FAO protein levels were increased in cardiac tissue, and FAO protein content was increased but FAO gene expression was unchanged in kidney tissue, suggesting that mRNA levels do not predict FAO capacity in liver, heart, and kidney tissue of Akita. Alternative mechanisms that regulate mitochondrial FAO protein content could include *1*) increased mRNA translation, *2*) decreased protein turnover, or *3*) increased import of proteins into the mitochondrion. Modulation of protein translation has been suggested in studies showing that hyperglycemia and hyperinsulinemia increase mRNA elongation and translation via dephosphorylation of eukaryotic elongation factor 2 in proximal tubular epithelial cells and that eukaryotic elongation factor 2 phosphorylation is reduced in renal cortex of type 2 diabetic *db/db* mice (27). Support also exists for the hypothesis that diabetes may regulate mitochondrial protein import in Akita. The translocase of the inner mitochondrial membrane 44 is induced in kidneys of streptozotocin-induced diabetic mice, and gene delivery of translocase of the inner mitochondrial membrane 44 increases mitochondrial import of manganese superoxide dismutase and glutathione reductase (28,29). Thus, future studies will be conducted to determine whether changes in the regulation of mRNA translation or mitochondrial import might regulate protein levels of FAO enzymes independently of changes in gene expression.

The TCA cycle and electron transport chain are important determinants of mitochondrial function. Since the proteome of these pathways was significantly remodeled in hepatic, cardiac, and renal mitochondria of Akita, we measured mitochondrial respiration and ATP synthesis rates. Despite the coordinate induction of OXPHOS subunits in liver mitochondria and the coordinate induction of TCA cycle enzymes in kidney mitochondria, state 3 respiration, FCCP-stimulated respiration, and ATP synthesis did not increase. The absence of differences in liver, brain or kidney mitochondrial function between Akita and nondiabetic controls could indicate a true absence of mitochondrial dysfunction in these tissues. It has to be acknowledged, though, that we investigated at a relatively early stage. Six weeks of diabetes might not have been sufficient to cause mitochondrial damage in liver, brain,

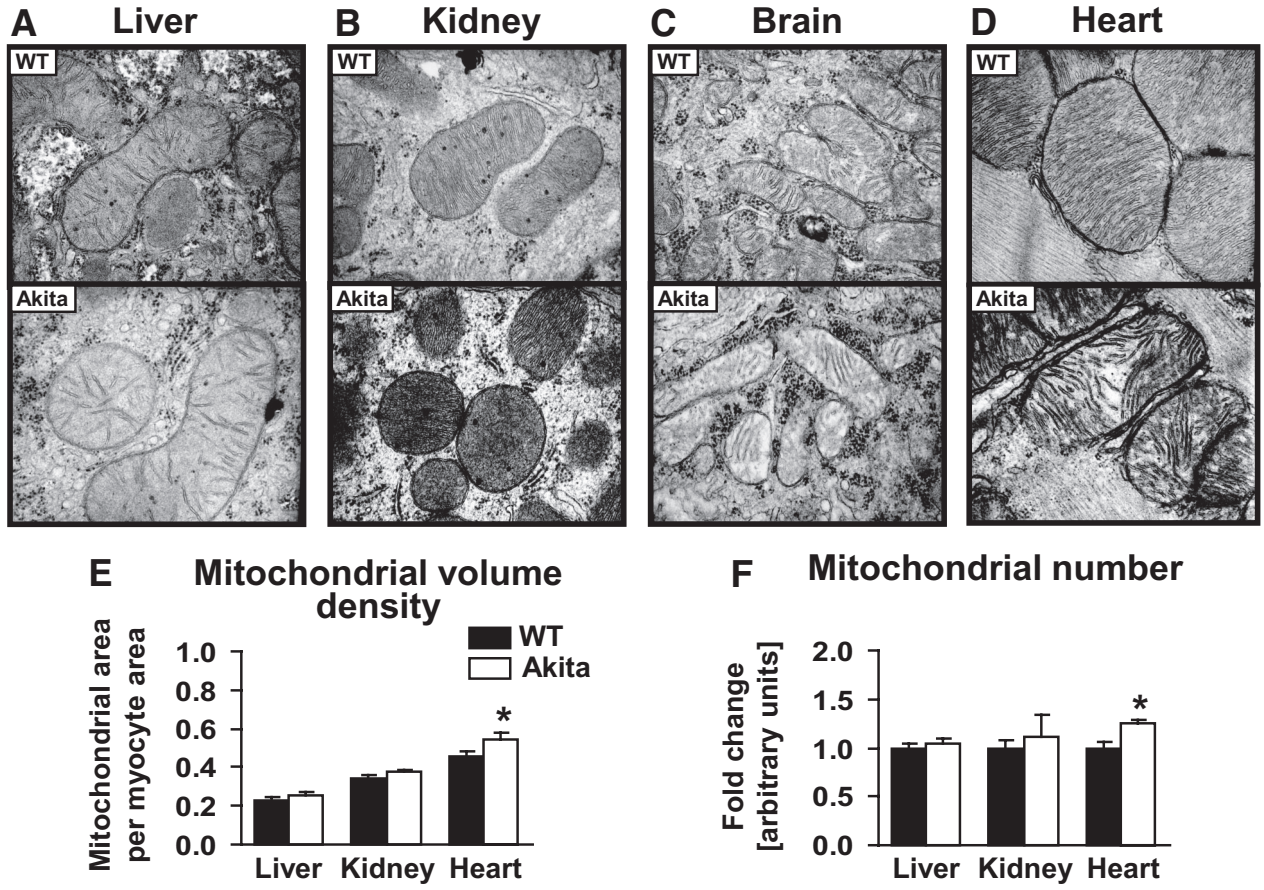

FIG. 6. Mitochondrial morphology. Representative longitudinal electron microscopy images of liver (*A*), kidney (*B*), brain (*C*), and heart (*D*) at a magnification of ×40,000 and quantification of mitochondrial volume density (*E*) and mitochondrial number (*F*), in liver, kidney, and heart tissue of 12-week-old wild-type (WT) (■) and Akita (□) mice ($n = 4$).

and kidney tissue, and whether a longer duration of diabetes could impair mitochondrial function in these tissues cannot be ruled out. Since insulin signaling may regulate mitochondrial function (30), low but measurable levels of insulin in the Akita mouse may partially offset the detrimental effect of diabetes and/or insulin deficiency on mitochondrial function in this model. Alternatively, the increase in protein content in certain mitochondrial pathways may reflect compensatory changes that offset impaired function elsewhere. Thus, the fact that proteomic changes do not reflect or predict actual metabolic flux rates in these tissues emphasizes the importance of using a systems biology approach including metabolite measurements (metabolomics) in combination with comparative proteomics to better inform the complex interaction of transcriptional and protein changes in the adaptation of mitochondria to diabetes. Our findings contrast with other studies that have reported impaired mitochondrial function in livers and kidneys of streptozotocin-induced diabetic models (5,8–10). Moreover, no impairment in mitochondrial morphology was observed in these tissues. Thus, the Akita model appears to be a unique model of type 1 diabetes that is relatively resistant to diabetes-induced mitochondrial damage in liver and kidney and may reflect the fact that these mice produce measurable amounts of insulin despite severe hyperglycemia (18).

In contrast to liver and kidney, mitochondrial function was impaired in Akita hearts using glutamate and succinate as substrates. Functional impairment was associated with reduced protein content of TCA cycle enzymes and OXPHOS subunits in Akita. At the gene level, mRNA content of four of five OXPHOS genes examined was reduced in Akita hearts, and there was a coordinate repression of the transcriptional regulators of mitochondrial mass and function (i.e., PGC-1α, PGC-1β, TFAm, and ERRα). Thus, these results suggest that reduced signaling via the PGC-1 transcriptional regulatory cascade may contribute to reduced TCA cycle and OXPHOS subunit content, leading to compromised mitochondrial function in Akita diabetic hearts. Oxidative damage unlikely contributes to reduced respiration rates since mitochondrial reactive oxygen species production and oxidative damage are not increased in hearts of the Akita mouse model (3). We cannot rule out that other mechanisms such as altered mitochondrial membrane lipid content or changes in glycosylation of mitochondrial proteins, which are proposed mechanisms for mitochondrial dysfunction in diabetes (31,32), may contribute to impaired cardiac mitochondrial function in Akita hearts. Based on the impairment in mitochondrial function and morphology, cardiac mitochondria appear to be affected to the greatest extent in 12-week-old type 1 diabetic Akita mice, relative to other tissues, underscoring an important role for mitochondrial dysfunction in cardiac complications of type 1 diabetes.

Analysis of the cardiac mitochondrial proteome revealed increased abundance of three FAO enzymes: long-chain acetyl-CoA dehydrogenase, acetyl-CoA acyltransferase 2, and hydroxyacyl-CoA dehydrogenase, all of which are essential components of the β-oxidation spiral. This induction is consistent with increased car-

diac FAO rates in the Akita mouse and other type 1 diabetic models (3,33). It is widely accepted that increased PPARα activity increases fatty acid oxidative capacity in diabetic hearts. Indeed, gene expression of PPARα and its target genes increases in streptozotocin-induced diabetic mice, and transgenic overexpression of PPARα in cardiomyocytes results in a metabolic phenotype similar to the diabetic heart (34). However, despite increased serum free fatty acid and triglyceride levels in the Akita mouse, expression of PPARα and its target gene medium-chain acyl CoA dehydrogenase was reduced in Akita hearts (3), suggesting either that increased FAO protein content may not be regulated by PPARα in Akita hearts or the existence of additional regulatory mechanisms that determine fatty acid oxidative capacity in Akita hearts, as discussed above.

In conclusion, tissue-specific remodeling of the proteome of mitochondrial energy metabolism in type 1 diabetic Akita mice was demonstrated. This remodeling was only partially mediated by transcriptional mechanisms. Despite remodeling of the mitochondrial proteome in all tissues investigated, impaired mitochondrial function was only observed in cardiac mitochondria, which we believe reflects greater repression of PGC-1α signaling in the heart relative to other tissues. These results confirm an important role of mitochondrial dysfunction in the pathogenesis of cardiac complications in type 1 diabetes.

ACKNOWLEDGMENTS

This work was supported by grants UO1HL70525 and UO1HL087947 from the National Institutes of Health and 19-2006-1071 from the Juvenile Diabetes Research Foundation to E.D.A., who is an Established Investigator of the American Heart Association. H.B. was supported by a postdoctoral fellowship grant from the German Research Foundation. C.R. was supported by fellowships from the Biomedical Sciences Exchange Program and the Erwin Riesch Foundation.

No potential conflicts of interest relevant to this article were reported.

REFERENCES

1. Borch-Johnsen K. The prognosis of insulin-dependent diabetes mellitus. An epidemiological approach. Dan Med Bull 1989;36:336–348
2. Dorman JS, Laporte RE, Kuller LH, Cruickshanks KJ, Orchard TJ, Wagener DK, Becker DJ, Cavender DE, Drash AL. The Pittsburgh insulin-dependent diabetes mellitus (IDDM) morbidity and mortality study: mortality results. Diabetes 1984;33:271–276
3. Bugger H, Boudina S, Hu XX, Tuinei J, Zaha VG, Theobald HA, Yun UJ, McQueen AP, Wayment B, Litwin SE, Abel ED. Type 1 diabetic akita mouse hearts are insulin sensitive but manifest structurally abnormal mitochondria that remain coupled despite increased uncoupling protein 3. Diabetes 2008;57:2924–2932
4. Yoon JC, Puigserver P, Chen G, Donovan J, Wu Z, Rhee J, Adelmant G, Stafford J, Kahn CR, Granner DK, Newgard CB, Spiegelman BM. Control of hepatic gluconeogenesis through the transcriptional coactivator PGC-1. Nature 2001;413:131–138
5. de Cavanagh EM, Ferder L, Toblli JE, Piotrkowski B, Stella I, Fraga CG, Inserra F. Renal mitochondrial impairment is attenuated by AT1 blockade in experimental type I diabetes. Am J Physiol Heart Circ Physiol 2008;294:H456–H465
6. Puigserver P, Spiegelman BM. Peroxisome proliferator-activated receptor-gamma coactivator 1 alpha (PGC-1 alpha): transcriptional coactivator and metabolic regulator. Endocr Rev 2003;24:78–90
7. Stanley WC, Lopaschuk GD, McCormack JG. Regulation of energy substrate metabolism in the diabetic heart. Cardiovasc Res 1997;34:25–33
8. Katyare SS, Satav JG. Effect of streptozotocin-induced diabetes on oxidative energy metabolism in rat kidney mitochondria: a comparative study of early and late effects. Diabetes Obes Metab 2005;7:555–562
9. Mastrocola R, Restivo F, Vercellinatto I, Danni O, Brignardello E, Aragno M, Boccuzzi G. Oxidative and nitrosative stress in brain mitochondria of diabetic rats. J Endocrinol 2005;187:37–44
10. Raza H, Prabu SK, Robin MA, Avadhani NG. Elevated mitochondrial cytochrome P450 2E1 and glutathione S-transferase A4–4 in streptozotocin-induced diabetic rats: tissue-specific variations and roles in oxidative stress. Diabetes 2004;53:185–194
11. Shen X, Zheng S, Thongboonkerd V, Xu M, Pierce WM Jr, Klein JB, Epstein PN. Cardiac mitochondrial damage and biogenesis in a chronic model of type 1 diabetes. Am J Physiol Endocrinol Metab 2004;287:E896–E905
12. Devi SS, Mehendale HM. Microarray analysis of thioacetamide-treated type 1 diabetic rats. Toxicol Appl Pharmacol 2006;212:69–78
13. Wilson KH, Eckenrode SE, Li QZ, Ruan QG, Yang P, Shi JD, Davoodi-Semiromi A, McIndoe RA, Croker BP, She JX. Microarray analysis of gene expression in the kidneys of new- and post-onset diabetic NOD mice. Diabetes 2003;52:2151–2159
14. Glyn-Jones S, Song S, Black MA, Phillips AR, Choong SY, Cooper GJ. Transcriptomic analysis of the cardiac left ventricle in a rodent model of diabetic cardiomyopathy: molecular snapshot of a severe myocardial disease. Physiol Genomics 2007;28:284–293
15. Turko IV, Murad F. Quantitative protein profiling in heart mitochondria from diabetic rats. J Biol Chem 2003;278:35844–35849
16. Johnson DT, Harris RA, French S, Aponte A, Balaban RS. Proteomic changes associated with diabetes in the BB-DP rat. Am J Physiol Endocrinol Metab 2009;296:E422–E432
17. Bolzan AD, Bianchi MS. Genotoxicity of streptozotocin. Mutat Res 2002;512:121–134
18. Yoshioka M, Kayo T, Ikeda T, Koizumi A. A novel locus, Mody4, distal to D7Mit189 on chromosome 7 determines early-onset NIDDM in nonobese C57BL/6 (Akita) mutant mice. Diabetes 1997;46:887–894
19. Hovius R, Lambrechts H, Nicolay K, de Kruijff B. Improved methods to isolate and subfractionate rat liver mitochondria. Lipid composition of the inner and outer membrane. Biochim Biophys Acta 1990;1021:217–226
20. Levin Y, Wang L, Ingudomnukul E, Schwarz E, Baron-Cohen S, Palotas A, Bahn S. Real-time evaluation of experimental variation in large-scale LC-MS/MS-based quantitative proteomics of complex samples. J Chromatogr B Analyt Technol Biomed Life Sci 2009;877:1299–1305
21. Champine PJ, Michaelson J, Weimer BC, Welch DR, DeWald DB. Microarray analysis reveals potential mechanisms of BRMS1-mediated metastasis suppression. Clin Exp Metastasis 2007;24:551–565
22. Boudina S, Sena S, Theobald H, Sheng X, Wright JJ, Hu XX, Aziz S, Johnson JI, Bugger H, Zaha VG, Abel ED. Mitochondrial energetics in the heart in obesity-related diabetes: direct evidence for increased uncoupled respiration and activation of uncoupling proteins. Diabetes 2007;56:2457–2466
23. Weibel E. Stereological principles for morphometry in electron microscopic cytology. Int Rev Cytol 1979;26:235–302
24. Johnson DT, Harris RA, French S, Blair PV, You J, Bemis KG, Wang M, Balaban RS. Tissue heterogeneity of the mammalian mitochondrial proteome. Am J Physiol Cell Physiol 2007;292:C689–C697
25. Mootha VK, Bunkenborg J, Olsen JV, Hjerrild M, Wisniewski JR, Stahl E, Bolouri MS, Ray HN, Sihag S, Kamal M, Patterson N, Lander ES, Mann M. Integrated analysis of protein composition, tissue diversity, and gene regulation in mouse mitochondria. Cell 2003;115:629–640
26. Rodgers JT, Lerin C, Haas W, Gygi SP, Spiegelman BM, Puigserver P. Nutrient control of glucose homeostasis through a complex of PGC-1alpha and SIRT1. Nature 2005;434:113–118
27. Sataranatarajan K, Mariappan MM, Lee MJ, Feliers D, Choudhury GG, Barnes JL, Kasinath BS. Regulation of elongation phase of mRNA translation in diabetic nephropathy: amelioration by rapamycin. Am J Pathol 2007;171:1733–1742
28. Wada J, Kanwar YS. Characterization of mammalian translocase of inner mitochondrial membrane (Tim44) isolated from diabetic newborn mouse kidney. Proc Natl Acad Sci U S A 1998;95:144–149
29. Zhang Y, Wada J, Hashimoto I, Eguchi J, Yasuhara A, Kanwar YS, Shikata K, Makino H. Therapeutic approach for diabetic nephropathy using gene delivery of translocase of inner mitochondrial membrane 44 by reducing mitochondrial superoxide production. J Am Soc Nephrol 2006;17:1090–1101
30. Boudina S, Bugger H, Sena S, O'Neill BT, Zaha VG, Ilkun O, Wright JJ, Mazumder PK, Palfreyman E, Tidwell TJ, Theobald H, Khalimonchuk O, Wayment B, Sheng X, Rodnick KJ, Centini R, Chen D, Litwin SE, Weimer BE, Abel ED. Contribution of impaired myocardial insulin signaling to mitochondrial dysfunction and oxidative stress in the heart. Circulation 2009;119:1272–1283
31. Ellis CE, Murphy EJ, Mitchell DC, Golovko MY, Scaglia F, Barcelo-Coblijn GC, Nussbaum RL. Mitochondrial lipid abnormality and electron transport chain impairment in mice lacking alpha-synuclein. Mol Cell Biol 2005;25:10190–10201

32. Hu Y, Suarez J, Fricovsky E, Wang H, Scott BT, Trauger SA, Han W, Hu Y, Oyeleye MO, Dillmann WH. Increased enzymatic O-GlcNAcylation of mitochondrial proteins impairs mitochondrial function in cardiac myocytes exposed to high glucose. J Biol Chem 2009;284:547–555
33. Sharma V, Dhillon P, Wambolt R, Parsons H, Brownsey R, Allard MF, McNeill JH. Metoprolol improves cardiac function and modulates cardiac metabolism in the streptozotocin-diabetic rat. Am J Physiol Heart Circ Physiol 2008;294:H1609–H1620
34. Finck BN, Lehman JJ, Leone TC, Welch MJ, Bennett MJ, Kovacs A, Han X, Gross RW, Kozak R, Lopaschuk GD, Kelly DP. The cardiac phenotype induced by PPARalpha overexpression mimics that caused by diabetes mellitus. J Clin Invest 2002;109:121–130